Section S1. The calculation method of collision efficiency between raindrops and aerosols

The three main collision mechanisms that underlie most theoretical derivations are Brownian diffusion E_{Bd}, directional interception E_{in}, and inertial impaction E_{im}. They were proposed by (Slinn, 1984) to calculate below-cloud wet scavenging coefficients (BWSCs), as shown in Eq. (1). These mechanisms did not consider all scavenging mechanisms, and therefore wet scavenging efficiency in the Greenfield gap was underestimated (Seinfeld and Pandis, 2006). In real atmospheric conditions, falling raindrops are also affected by fluctuating turbulence, raindrop evaporation, particle fragmentation and particle charges (Wang et al., 2010). Turbulence, as well as raindrop evaporation and fragmentation, can increase the concentrations of raindrops and aerosol particles and so increase collision efficiency, which can have great influences on below-cloud wet scavenging mechanisms. Based on the previous laboratory research and theoretical derivation methods, thermophoresis E_{th} , diffusiophoresis E_{di} and electrostatic interaction E_{es} are added, as shown in Eq. (S2). The equations of the six mechanisms are summarized in Table S2.

$$E\left(D_p, d_p\right)_{traditional} = E_{Bd} + E_{in} + E_{im} \qquad (S1)$$

$$E\left(D_p, d_p\right)_{new} = E\left(D_p, d_p\right)_{traditional} + E_{th} + E_{di} + E_{es} \qquad (S2)$$

The semi-empirical parameterized characterization of Brownian diffusion is (Slinn, 1984):

$$E_{Bd} = \frac{4}{ReSc}\left(1 + 0.4Re^{\frac{1}{2}}Sc^{\frac{1}{3}} + 0.16Re^{\frac{1}{2}}Sc^{\frac{1}{2}}\right) \qquad (S3)$$

where $Re = \frac{D_p U(D_p)\rho_a}{2\mu_a}$, $Sc = \frac{\mu_a}{\rho_a D_{diff}}$, and vapor diffusivity $D_{diff} = \frac{k_b T C_c}{3\pi\mu_a d_p}$; k_b is the Boltzmann's constant, and $C_c = 1 + \frac{2\lambda}{d_p}[1.257 + 0.4exp(-\frac{0.55d_p}{\lambda})]$ that is Cunningham correction coefficients.

Directional interception is given by:

$$E_{in} = 4\frac{d_p}{D_p}[w + \left(1 + 2Re^{\frac{1}{2}}\right)\left(\frac{d_p}{D_p}\right) \qquad (S4)$$

where $w = \frac{\mu_a}{\mu_w}$, μ_a and μ_w are the atmospherics and raindrop viscosity, respectively.

Inertial impaction is calculated by

$$E_{im} = [\frac{St - St^*}{St - St^* + \frac{2}{3}}]^{\frac{3}{2}} \quad (S5)$$

where $St = \frac{2\tau U(D_p)}{D_p}$. τ is relaxation time that $\tau = \frac{(\rho_p - \rho_a) d_p^2 C_c}{18\mu_a}$ and $St^* = \frac{1.2 + ln(1+Re)/12}{1 + ln(1+Re)}$ is the characteristic Stokes constant.

Thermophoresis is calculated according to Davenport and Peters (Davenport and Peters, 1978):

$$E_{th} = \frac{4\alpha\left(2 + 0.6Re^{\frac{1}{2}}Pr^{\frac{1}{3}}\right)(T - T_s)}{U(D_p)D_p} \quad (S6)$$

where $\alpha = \frac{2C_c(k_a + 5\lambda k_p/d_p)k_a}{5P(1+6\lambda/d_p)(2k_a + k_p + 10\lambda k_p/d_p)}$, and $Pr = \frac{C_p \mu_a}{k_a}$. The thermal conductivity of atmospheric and aerosol particles is closely related to temperature, whose semi-empirical formulae are $k_a = 2k_p$ and $k_a = 1.5207 \times 10^{-11}T^3 - 4.8574 \times 10^{-8}T^2 + 1.0184 \times 10^{-4}T - 3.9333 \times 10^{-4}$, respectively (Bae et al., 2009).

Differs from thermophoresis, diffusiophoresis occurs because of the movement of aerosol particles due to the concentration gradient of the aerosol mixture. The calculation of diffusiophoresis is given by (Bae et al., 2009):

$$E_{di} = \frac{4\beta\left(2 + Re^{\frac{1}{2}}Scw^{\frac{1}{3}}\right)\left(\frac{p_s^0}{T_s} - \frac{p^0 RH}{T}\right)}{U(D_p)D_p} \quad (S7)$$

where $\beta = \frac{TD_w}{P}(\frac{M_w}{M_a})^{1/2}$; $Scw = \frac{\mu_a}{\rho_a D_w}$ is Schmidt number of water vapor, $D_w = 0.211(\frac{T}{273.15})(\frac{1.0132\times10^6}{P}$ is the diffusivity of water vapor. Vapor pressure (p^0) at atmospheric temperature T and vapor pressure (p_s^0) at the surface temperature of a raindrop (T_s) are given by (Seinfeld and Pandis, 2006): $p^0 = 1.0132 \times 10^6 exp(13.3185a - 1.97a^2 - 0.6445a^3 - 0.1299a^4)$, where $a = 1 - \frac{373.15}{T}$, and

$p_s^0 = 1.0132 \times 10^6 exp(13.3185a_s - 1.97a_s^2 - 0.6445a_s^3 - 0.1299a_s^4)$, where $a_s = 1 - \frac{373.15}{T_s}$, respectively.

Andronache (2004a) found that collection efficiency due to charge effect exists between raindrops and aerosol particles. It was assumed that the charges of raindrops Q and aerosol particles q were opposite. Under this assumption, aerosol particles are easily captured by electrostatic interaction when close to the falling streamline of the raindrop surface. Electrostatic interaction mostly occurs in the case of charged cloud precipitation, often accompanied by heavy precipitation weather. Collision efficiency generated by electrostatic interaction is given by Davenport and Peters (1978):

$$E_{es} = \frac{16KC_cQq}{3\pi\mu_a U(D_p)D_p^2 d_p} \qquad (S8)$$

where $Q = a\alpha D_p^2$ and $q = a\alpha d_p^2$ are the average electrification of raindrops and aerosol particles, respectively. Generally, a is a constant with value of 0.83×10^{-6}. α is an empirical parameter ($C\cdot m^{-2}$) with the general range from 0 to 7. According to previous observation results, 0 represents neutral and 7 occurs in the case of conductive charging. Generally, α is set as 2 which characterizes the average charge intensity (Pruppacher and Klett, 1997).

Section S2. The observational method of raindrop size distribution in Beijing

A laser raindrop spectrograph (OTT Parsivel 2, Germany) was used for field observation for one year (August 2017 to July 2018) to measure precipitation parameters. The laser raindrop spectrograph was located 700 m east of the tower of the Institute of Atmospheric Physics (IAP, 39°58′28″N, 116°22′1″E), Chinese Academy of Sciences, Beijing. The central sampling area of the laser raindrop spectrograph was 180 mm×30 mm, and the sampling interval was 60 s. There were 32 non-isometric velocity channels and 32 particle diameter channels with ranges of 0.2~20.8 m s^{-1} and 0.25~25 mm, respectively.

In order to eliminate the influences of external environment and any instruments, the observed raindrop spectra requires quality control and these data are removed: The first two particle diameter channels and any raindrops with a particle diameter greater than 8 mm; results with a particle count of less than 10; and data for which deviation between the observed velocity and the calculation results of empirical formula from Atlas et al. Atlas et al. (1973) is greater than 5 m s^{-1} (Xiong, 2016). After quality control, the raindrop spectrum is calculated with the particle numbers in each channel ($\triangle D_p$):

$$N(D_p)(mm \cdot m^{-3}) = \frac{n(D_p) \times 10000cm^2 \cdot m^{-2}}{U_t(D_p)(m \cdot s^{-1}) \times \triangle D_p(mm) \times 54 \times 60s} \quad (S9)$$

Where $U_t(D_p)$ is calculated by the equation of raindrop terminal velocity given by Atlas et al. (1973).

Section S3. The measurement of BWSCs in Beijing

The measurement site is located on top of the two-floor building of the Institute of Atmospheric Physics (IAP, 39°58′28″N, 116°22′1″E) between the north 3rd and 4th Ring Road of Beijing, China. It is a typical urban site with long-term observation of aerosols components as well as the rainfall sampling for offline analysis (Sun et al., 2015; Xu et al., 2019; Xu et al., 2017). Hourly data of $PM_{2.5}$ compositions were observed by an Ambient Ion Monitor-Ion Chromatograph (AIM-IC) developed by URG Corp., Chapel Hill, NC and Dionex Inc., Sunnyvale, CA, in 2014 (Xu et al., 2017) and in the Atmospheric Pollution and Human Health Beijing (APHH-Beijing) campaign of 2016 (Xu et al., 2019). The rainfall sampling of every event was performed using an automatic wet-dry sampler. After that, the samples were refrigerated at 0~4℃ and analyzed in a laboratory within one month, following the same procedure used for the Acid Rain Monitoring Network run by the China Meteorological Administration (Tang et al., 2010). Nine ions of SO_4^{2-}, NO_3^-, Cl^-, F^-, NH_4^+, Na^+, K^+, Ca^{2+} and Mg^{2+} were quantitatively measured by using ion chromatography (IC, Dionex 600, USA). More detailed description on the measurement of $PM_{2.5}$ compositions and the chemical ions in precipitation can be found in Xu et al. (2017). Besides, the partical size distribution from 14 nm to 740 nm and from 0.4~10.35 μm were also measured by a scanning mobility particle sizer (SMPS) and a polarization optical particle counter (POPC), respectively. A single-particle aerosol mass spectrometer (SPAMS) was also deployed during the APHH-Beijing winter campaign in China National Environmental Monitoring Center, which is located in the northeast, 8 km away from the IAP sampling site to obtain the chemical compositions with aerosol diameters ranging from 0.2 μm to 2.5 μm. More detailed description can be found in Xu et al. (2019).

The existing approaches based on field observations to estimate BWSCs including the followings. One approach is based on the change in the number concentration of aerosols, called O1:

$$K(d_p) = \frac{1}{t_1 - t_0} \ln \left[\frac{N_0(d_p)}{N_1(d_p)}\right] \quad (S10)$$

where $N_0(d_p)$ and $N_1(d_p)$ are the measured aerosol particle number concentrations before the rain occurs (t_0) and after the rain ends (t_1), respectively (Laakso et al., 2003). The second is estimated by the bulk model based on the aerosol mass balance within a certain bulk, which assumes that there is a box with a horizontal area and vertical height above the observation site, called O2:

$$K = \frac{C_p}{C_a(0) \times f} \times \frac{P}{h} \qquad (S11)$$

where C_p and $C_a(0)$ are the paired aerosol concentrations in the precipitation and aerosol at the surface, h is the cloud-base height during rainfall, and $f = \frac{\sum_{z=0}^{h} \frac{C_a(z)}{C_a(0)} \times h\prime(z)}{\sum_{z=0}^{h} h\prime(z)}$ is the vertical distribution factor of aerosols (Andronache, 2004b; Okita et al., 1996). The third is an improved method based on O2, called as O2':

$$K = \frac{C_{p,below}}{C'_a(0) \times f} \times \frac{P}{h} \qquad (S12)$$

where $C_{p,below}$ is the washout concentration that have been eliminated the rainwater concentrations in each increment and $C_a'(0)$ is the aerosol concentration at the surface that considered the cleansing effects of prevailing wind in Beijing from north and north-west (Xu et al., 2019).

Table S1. Physical parameterization schemes employed in WRF

Physics schemes	Options
Microphysics scheme	Predicted Particle Property scheme (Morrison and Milbrandt, 2015)
Longwave radiation scheme	RRTMG scheme (Iacono et al., 2008)
Shortwave radiation scheme	Goddard shortwave scheme (Chou and Suarez, 1994)
Planetary boundary layer scheme	Yonsei University scheme (Hong et al., 2006)
Surface layer scheme	MM5 similarity scheme (Jiménez et al., 2012)
Land surface scheme	Noah land surface model scheme (Chen and Dudhia, 2001)
Cumulus parameterization scheme	Grell 3D scheme (Grell, 1993; Grell and Dévényi, 2002)

Table S2. List of formulas for raindrop and aerosol collision efficiencies and wet scavenging coefficient

Wet scavenging coefficient and collision mechanisms			Equations	Range of value
Collision mechanisms	Conventional collision mechanism (Seinfeld and Pandis, 2006; Slinn, 1984)	Brownian diffusion	$E_{Bd} = \frac{4}{ReSc}(1 + 0.4Re^{1/2}Sc^{1/3} + 0.16Re^{1/2}Sc^{1/2})$	10^{-5}~10^{-1}
		Directional interception	$E_{in} = 4\frac{d_p}{D_p}[w + (1 + 2Re^{1/2})(\frac{d_p}{D_p})]$	10^{-6}~10^{-2}
		Inertial impaction	$E_{im} = [\frac{St - St^*}{St - St^* + \frac{2}{3}}]^{\frac{3}{2}}$	10^{-6}~10^{0}
	Thermophoresis (Bae et al., 2009)		$E_{th} = \frac{4\alpha(2 + 0.6Re^{1/2}Pr^{1/3})(T - T_s)}{U(D_p)D_p}$	10^{-4}~10^{-3}
	Diffusiophoresis (Bae et al., 2009)		$E_{di} = \frac{4\beta(2 + Re^{1/2}Scw^{1/3})(\frac{p_s^0}{T_s} - \frac{p^0 RH}{T})}{U(D_p)D_p}$	10^{-4}~10^{-3}
	Electrostatic interaction (Andronache, 2004a; Wang et al., 2010)		$E_{es} = \frac{16KC_cQq}{3\pi\mu_a U(D_p)D_p^2 d_p}$	10^{-4}~10^{-2}
Wet scavenging coefficient	CAMx (Environ.Inc, 2013)		$\Lambda = 4.2 \times 10^{-7}\frac{EP}{D_p}$	10^{-7}~10^{-4} (BWSC)
	Ge14 (Ge et al., 2014)		$\Lambda = \left(\frac{\overline{W_T}\Delta Z_{cld}}{\rho_w P}\right)^{-1}$	10^{-4}~10^{-2}

Notes: For wet scavenging coefficient of CAMx, E is the collision efficiency, P is the precipitation rate, D_p is the raindrop diameter. For wet scavenging coefficient of Ge14, ΔZ_{cld} is the cloud thickness, $\overline{W_T}$ is the mean total water content, ρ_w is the density of water.

Table S3. The basic information of atmospheric nitrogen wet deposition observational sites

Longitude	Latitude	Country	Longitude	Latitude	Country
116.46	39.92	China	114.82	30.38	China
117.20	39.13	China	112.19	31.02	China
114.48	38.03	China	112.23	30.30	China
118.02	39.63	China	114.28	29.87	China
119.57	39.95	China	113.00	28.21	China
114.47	36.60	China	113.16	27.83	China
115.48	38.85	China	112.91	27.87	China
114.87	40.82	China	113.09	29.37	China
117.93	40.97	China	111.69	29.05	China
116.83	38.33	China	110.48	29.13	China
116.70	39.53	China	112.33	28.60	China
115.72	37.72	China	113.00	25.79	China
112.53	37.87	China	111.63	26.40	China
113.3	40.12	China	109.95	27.52	China
113.57	37.85	China	111.96	27.71	China
113.08	36.18	China	113.23	23.16	China
112.42	39.32	China	113.62	24.84	China
112.72	37.68	China	114.07	22.62	China
110.97	35.03	China	113.52	22.30	China
111.65	40.82	China	116.69	23.39	China
110.00	40.58	China	113.11	23.05	China
118.87	42.28	China	110.38	21.20	China
122.28	43.63	China	110.88	21.68	China
119.73	49.22	China	112.44	23.05	China
113.08	41.03	China	114.40	23.09	China
123.38	41.80	China	111.95	21.85	China
121.62	38.92	China	113.75	23.04	China
122.85	41.12	China	113.38	22.52	China
123.97	41.97	China	116.63	23.68	China
124.37	40.13	China	116.35	23.55	China

121.15	41.13	China	112.02	22.93	China
122.18	40.65	China	110.28	25.29	China
121.65	42.00	China	111.34	23.51	China
123.17	41.28	China	109.12	21.49	China
122.05	41.19	China	108.61	21.96	China
123.85	42.32	China	110.14	22.64	China
120.83	40.77	China	106.62	23.91	China
125.35	43.88	China	108.06	24.70	China
126.57	43.87	China	110.35	20.02	China
126.63	45.75	China	109.50	18.25	China
121.26	31.13	China	106.54	29.59	China
118.78	32.04	China	104.75	29.35	China
120.29	31.59	China	101.75	26.61	China
120.26	31.91	China	105.39	28.91	China
119.82	31.36	China	104.37	31.13	China
117.20	34.26	China	104.73	31.48	China
119.95	31.79	China	105.86	32.44	China
120.62	31.32	China	105.04	29.59	China
120.86	32.01	China	103.73	29.59	China
120.45	32.57	China	103.81	30.05	China
121.18	32.33	China	104.56	28.77	China
121.66	31.80	China	107.05	31.22	China
120.56	32.39	China	102.97	29.97	China
121.15	31.89	China	104.60	30.19	China
119.16	34.59	China	102.29	27.92	China
119.15	33.50	China	104.82	26.58	China
120.13	33.38	China	106.90	27.70	China
120.31	32.84	China	109.21	27.73	China
119.42	32.39	China	107.53	26.72	China
119.44	32.20	China	102.73	25.04	China
119.55	32.00	China	103.79	25.51	China
119.81	32.24	China	99.18	25.12	China
119.90	32.49	China	103.70	27.32	China
119.82	32.93	China	101.54	25.01	China

118.79	34.12	China	102.43	23.35	China
118.68	33.73	China	109.11	35.09	China
120.19	30.26	China	108.72	34.36	China
121.56	29.86	China	109.50	34.52	China
120.65	28.01	China	109.47	36.60	China
120.76	30.77	China	102.24	38.50	China
120.10	30.86	China	107.60	35.73	China
120.58	30.01	China	101.74	36.56	China
119.64	29.12	China	106.27	38.47	China
118.88	28.97	China	106.39	39.04	China
122.10	30.04	China	87.68	43.77	China
121.43	28.55	China	84.77	45.59	China
117.27	31.86	China	87.31	44.05	China
118.38	31.33	China	82.10	44.93	China
117.34	32.93	China	80.29	41.15	China
116.98	32.62	China	81.33	43.91	China
118.48	31.56	China	84.89	44.45	China
116.77	33.97	China	85.94	44.27	China
117.82	30.92	China	104.83	11.55	Cambodia
117.03	30.52	China	106.50	29.62	China
118.13	30.28	China	106.37	29.82	China
118.31	32.33	China	108.95	34.23	China
115.81	32.89	China	108.80	33.83	China
116.97	33.63	China	118.13	24.47	China
115.75	33.86	China	118.03	24.85	China
117.48	30.66	China	113.50	22.27	China
118.76	30.95	China	106.83	-6.18	Indonesia
119.30	26.08	China	106.57	-6.25	Indonesia
118.10	24.46	China	100.32	-0.20	Indonesia
117.61	26.23	China	107.58	-6.90	Indonesia
118.58	24.93	China	119.57	-4.92	Indonesia
118.16	26.65	China	141.21	45.12	Japan
117.01	25.12	China	140.35	41.25	Japan
119.52	26.65	China	138.40	38.25	Japan

115.89	28.68	China	137.80	36.70	Japan
117.22	29.30	China	136.69	35.57	Japan
113.85	27.60	China	133.19	36.29	Japan
115.97	29.71	China	131.80	34.68	Japan
114.92	27.81	China	132.93	33.38	Japan
117.02	28.23	China	128.25	26.87	Japan
114.92	25.85	China	142.22	27.09	Japan
114.97	27.12	China	139.76	35.69	Japan
114.38	27.81	China	101.65	3.10	Malaysia
117.00	36.65	China	101.38	4.47	Malaysia
118.05	36.78	China	117.85	4.98	Malaysia
117.57	34.86	China	110.47	1.48	Malaysia
118.49	37.46	China	96.12	16.50	Myanmar
121.39	37.52	China	121.07	14.63	Philippines
119.10	36.62	China	120.6	16.42	Philippines
116.59	35.38	China	126.28	37.70	Korea
117.13	36.18	China	126.16	33.30	Korea
122.10	37.50	China	127.18	35.60	Korea
119.46	35.42	China	101.00	51.67	Russia
117.67	36.19	China	104.90	51.85	Russia
118.35	35.05	China	104.25	52.23	Russia
116.29	37.45	China	132.12	43.70	Russia
118.03	37.36	China	100.53	13.77	Tailand
115.43	35.24	China	100.57	13.73	Tailand
113.65	34.76	China	100.77	14.03	Tailand
114.35	34.79	China	98.58	14.77	Tailand
112.44	34.70	China	98.93	18.77	Tailand
113.29	33.75	China	101.88	14.45	Tailand
113.21	35.24	China	105.85	21.02	Vietnam
112.57	35.08	China	105.33	20.82	Vietnam
114.31	30.52	China	105.72	20.25	Vietnam
115.09	30.20	China	108.21	16.04	Vietnam
110.79	32.65	China	105.69	10.08	Vietnam
111.30	30.70	China	106.70	10.78	Vietnam

112.20	32.08	China			

Table S4. The basic information of the sites for comparison of five major atmospheric reactive nitrogen (N_r) species from NNDMN

Stations	Longitude	Latitude
China Agricultural Unviversity	116.28	40.02
Zhengzhou	113.37	34.75
Dalian	121.58	38.92
Baiyun	113.27	23.16
Wenjiang	103.84	30.55
Shangzhuang	116.20	40.11
Yangqu	112.89	38.05
Zhumadian	114.05	33.02
Yangling	108.01	34.31
Yucheng	116.63	36.94
Gongzhuling	124.83	43.53
Lishu	124.17	43.36
Wuwei	102.60	38.07
Wuxue	115.79	30.01
Taojiang	111.97	28.61
Fengyang	117.56	32.88
Zhanjiang	110.33	21.26
Fuzhou	119.36	26.17
Fenghua	121.53	29.61
Ziyang	104.63	30.13
Jiangjin	106.18	29.06
Lingshadao	120.18	35.77
Changdao	120.75	37.93
Duolun	116.49	42.20
Feiyue	113.34	28.56
Huinong	113.41	28.52
Xishan	113.31	28.61

Table S5. The validation results of high annually averaged concentration in precipitation in Region I of the four wet deposition schemes

Metrics	Obs. TIN>3.0mgN L^{-1} （N=41）			
	CAMx	Ge14	Ge14-CAMx	Ge14-BWSC
MM	3.19	5.49	3.49	4.29
MO	4.47	4.47	4.47	4.47
R	0.40	0.35	0.39	0.37
NMB	-29%	23%	-22%	-4%
NME	31%	36%	27%	23%
RMSE	1.70	2.18	1.53	1.51

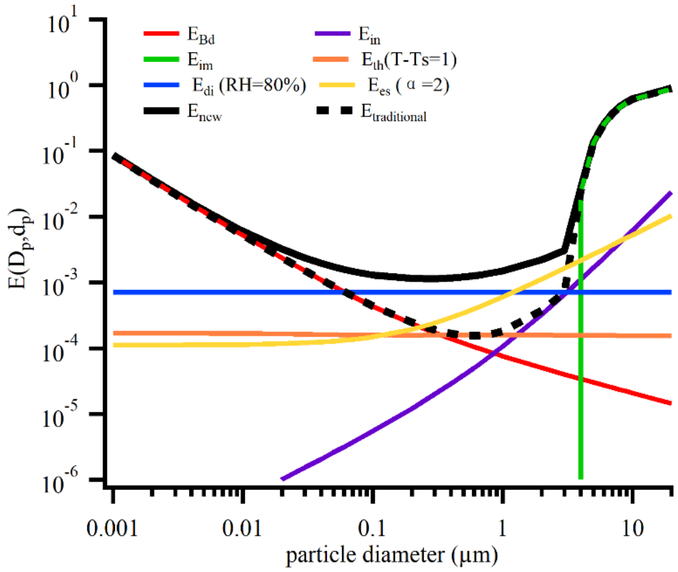

Figure S1. Variation of collection efficiency $E(D_p,d_p)_{traditional}$ by Brownian diffusion, directional interception, and inertial impaction (dotted line) and updated collection efficiency $E(D_p,d_p)_{new}$ adding the thermophoretic, diffusiophoretic and electrostatic mechanism (solid line). The setting parameters are based on standard atmospheric pressure, a precipitation rate of 10 mm h^{-1}, an empirical electrostatic parameter α of 2, an ambient temperature of 30℃, a raindrop-to-ambient temperature difference of 3, and a relative humidity of 80%.

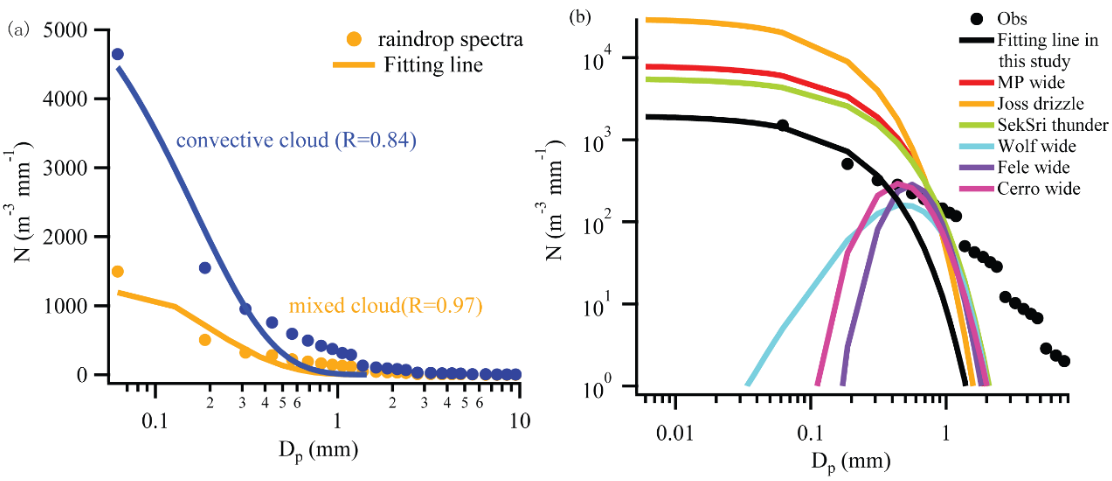

Figure S2. (a) Raindrop size distribution of convective and mixed cloud precipitation during 2017.8~2018.7 and (b) comparison with previous studies.

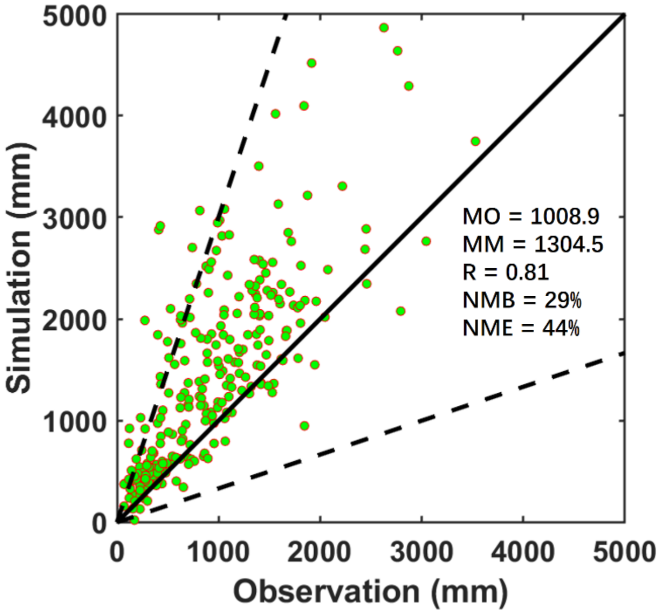

Figure S3. Validation of annual precipitation.

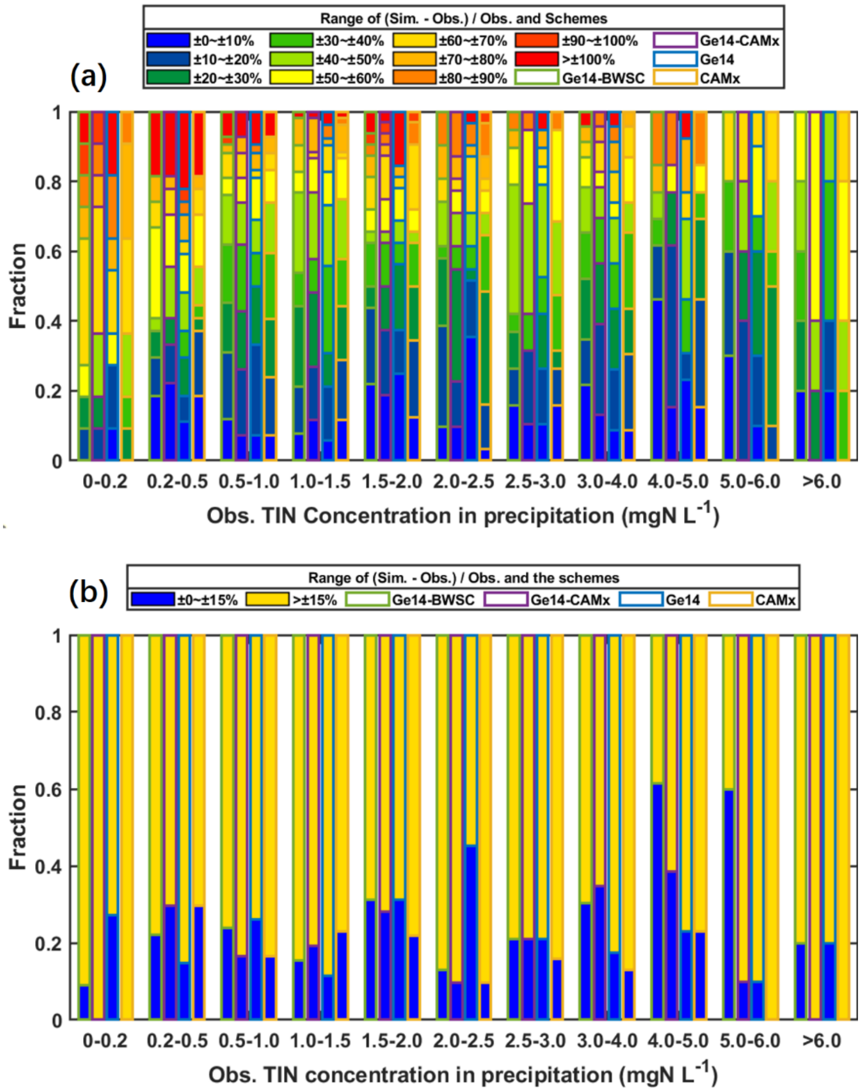

Figure S4. Comparison of performance of the four schemes across observed annual mean TIN concentration in precipitation intervals.

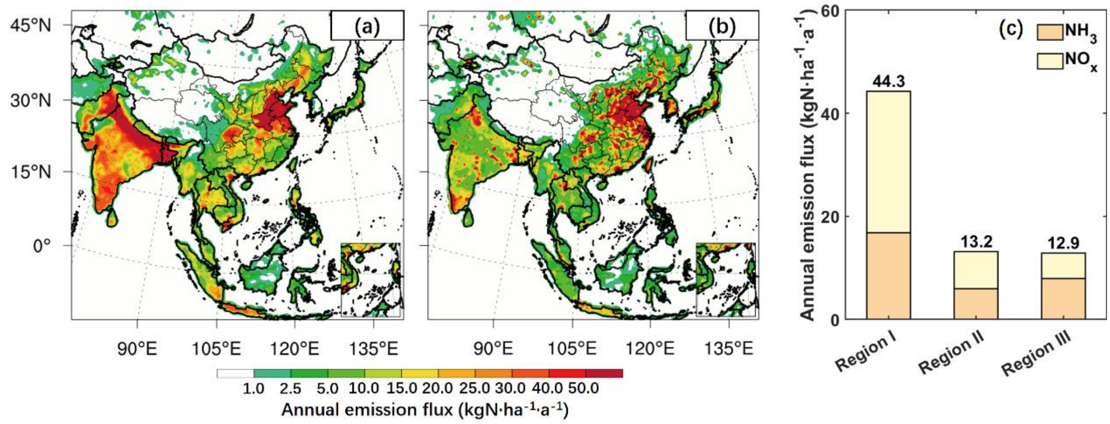

Figure S5. The annual emission fluxes of (a) NH_3 and (b) NO_x, and (c) the average emission flux of them in Region I, II and III.

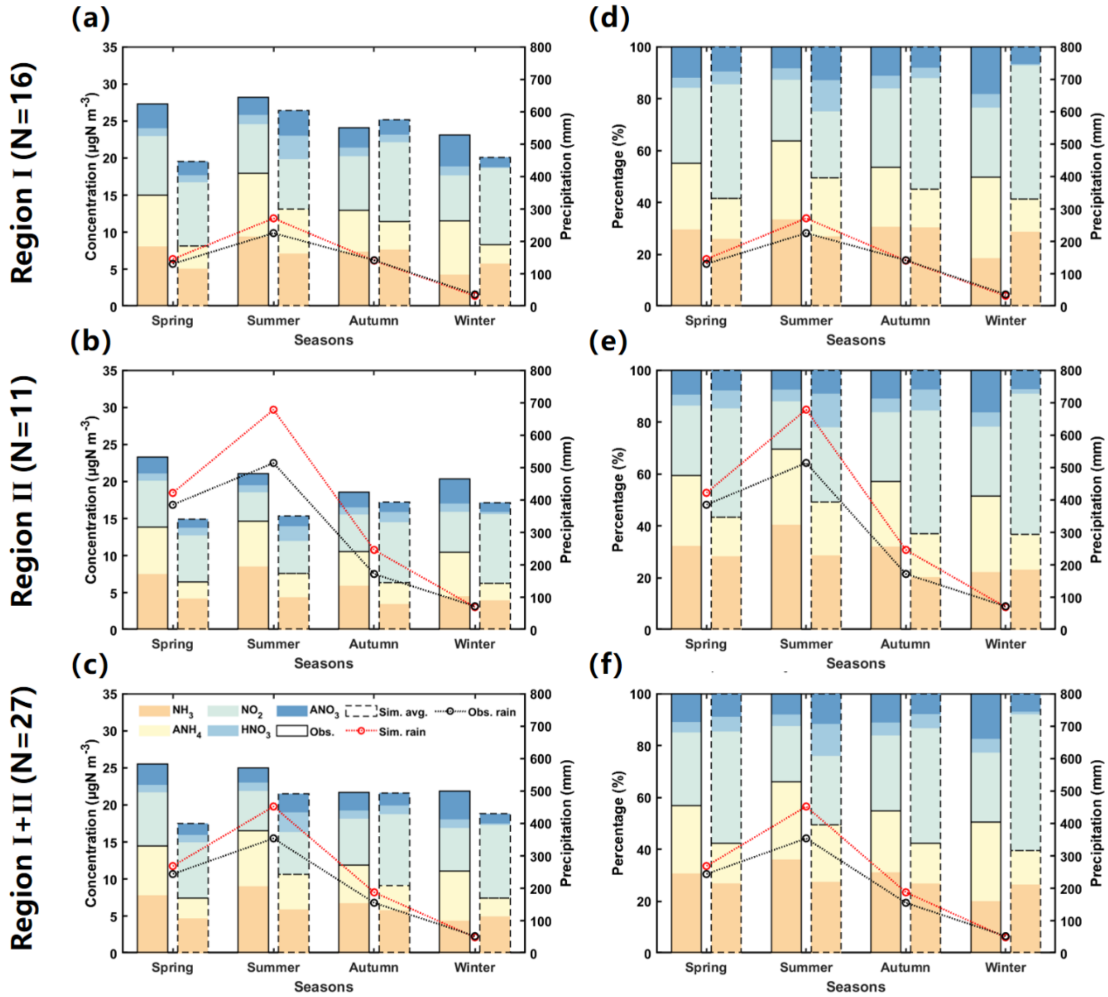

Figure S6. Comparison between the observation and the simulation of average of the four wet deposition schemes on atmospheric N_r concentrations.

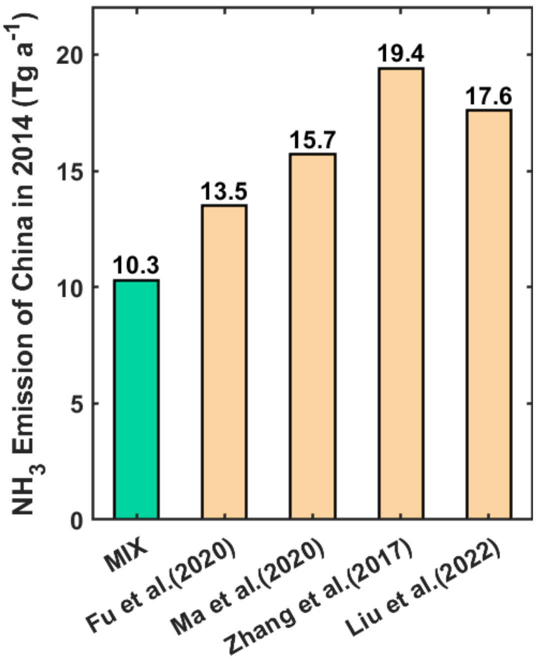

Figure S7. Comparison of NH_3 emission of China in 2014 between the MIX inventory and other studies (Fu et al., 2020; Liu et al., 2022; Ma, 2020; Zhang et al., 2017).

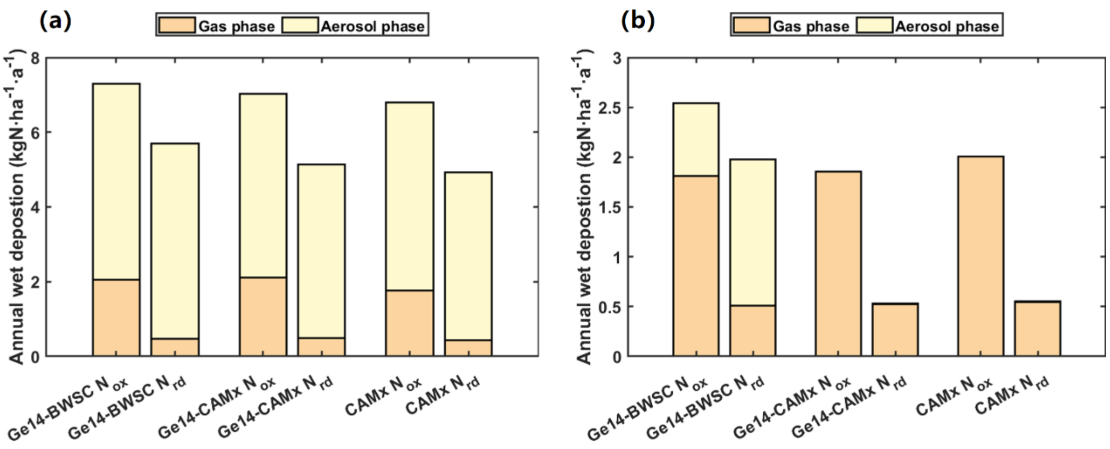

Figure S8. The simulated annual (a) in-cloud and (b) below-cloud deposition of gas and aerosol in N_{ox} and N_{rd} for the Ge14-BWSC, Ge14-CAMx and CAMx schemes. The gas is mainly HNO_3 in N_{ox} and NH_3 in N_{rd}. The in-cloud and below-cloud deposition is based on the simulated results at the observational sites by the three schemes.

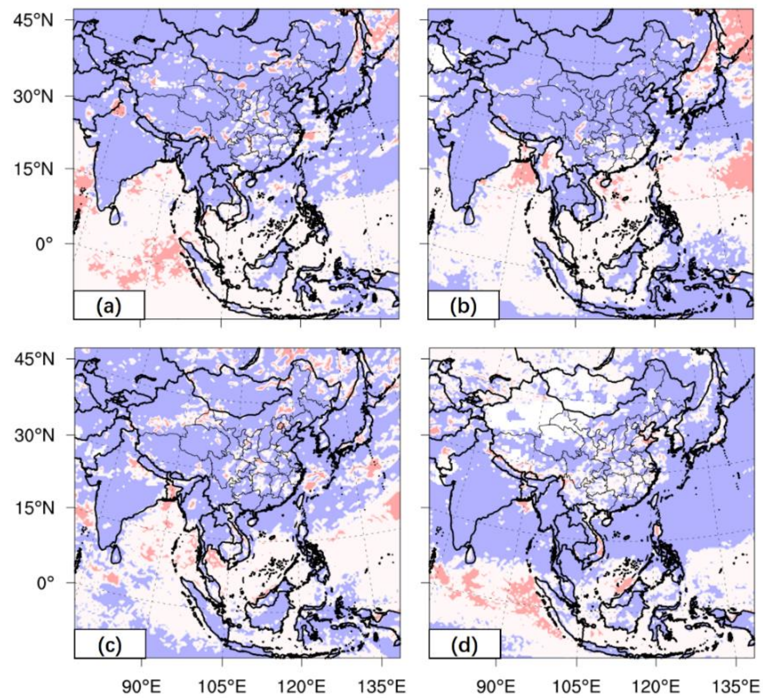

Figure S9. The seasonal difference pattern between the Ge14-BWSC and Ge14-CAMx schemes on TIN wet deposition.

References

Andronache, C.: Diffusion and electric charge contributions to below-cloud wet removal of atmospheric ultra-fine aerosol particles, J. Aerosol. Sci., 35, 1467-1482, 10.1016/j.jaerosci.2004.07.005, 2004a.

Andronache, C.: Estimates of sulfate aerosol wet scavenging coefficient for locations in the Eastern United States, Atmos. Environ., 38, 795-804, 10.1016/j.atmosenv.2003.10.035, 2004b.

Atlas, D., Srivastava, R. C., and Sekhon, R. S.: Doppler radar characteristics of precipitation at vertical incidence, Rev. Geophys., 11, 1-35, 10.1029/RG011i001p00001, 1973.

Bae, S. Y., Jung, C. H., and Kim, Y. P.: Relative contributions of individual phoretic effect in the below-cloud scavenging process, J. Aerosol. Sci., 40, 621-632, 10.1016/j.jaerosci.2009.03.003, 2009.

Chen, F. and Dudhia, J.: Coupling an advanced land surface-hydrology model with the Penn State-NCAR MM5 modeling system. Part I: Model implementation and sensitivity, Mon. Weather Rev., 129, 569-585, 10.1175/1520-0493(2001)129<0569:Caalsh>2.0.Co;2, 2001.

Chou, M.-D. and Suarez, M. J.: An efficient thermal infrared radiation parameterization for use in general circulation models, 1994.

Davenport, H. M. and Peters, L. K.: Field studies of atmospheric particulate concentration changes during precipitation, Atmos. Environ., 12, 997-1008, 10.1016/0004-6981(78)90344-x, 1978.

ENVIRON.INC: User's Guide Comprehensive Air Quality Model with Extensions (CAMx) Version 6, 773 San Marin Drive, Suite 2115, Novato, California, 310 pp.2013.

Fu, H., Luo, Z. B., and Hu, S. Y.: A temporal -spatial analysis and future trends of ammonia emissions in China, Science of the Total Environment, 731, 9, 10.1016/j.scitotenv.2020.138897, 2020.

Ge, B. Z., Wang, Z. F., Xu, X. B., Wu, J. B., Yu, X. L., and Li, J.: Wet deposition of acidifying substances in different regions of China and the rest of East Asia:

Modeling with updated NAQPMS, Environ. Pollut., 187, 10-21, 10.1016/j.envpol.2013.12.014, 2014.

Grell, G. A.: Prognostic evaluation of assumptions used by cumulus parameterizations, Mon. Weather Rev., 121, 764-787, 10.1175/1520-0493(1993)121<0764:Peoaub>2.0.Co;2, 1993.

Grell, G. A. and Dévényi, D.: A generalized approach to parameterizing convection combining ensemble and data assimilation techniques -: art. no. 1693, Geophys. Res. Lett., 29, 4, 10.1029/2002gl015311, 2002.

Hong, S. Y., Noh, Y., and Dudhia, J.: A new vertical diffusion package with an explicit treatment of entrainment processes, Mon. Weather Rev., 134, 2318-2341, 10.1175/mwr3199.1, 2006.

Iacono, M. J., Delamere, J. S., Mlawer, E. J., Shephard, M. W., Clough, S. A., and Collins, W. D.: Radiative forcing by long-lived greenhouse gases: Calculations with the AER radiative transfer models, J. Geophys. Res.-Atmos., 113, 8, 10.1029/2008jd009944, 2008.

Jiménez, P. A., Dudhia, J., González-Rouco, J. F., Navarro, J., Montávez, J. P., and García-Bustamante, E.: A Revised Scheme for the WRF Surface Layer Formulation, Mon. Weather Rev., 140, 898-918, 10.1175/mwr-d-11-00056.1, 2012.

Laakso, L., Grönholm, T., Rannik, Ü., Kosmale, M., Fiedler, V., Vehkamäki, H., and Kulmala, M.: Ultrafine particle scavenging coefficients calculated from 6 years field measurements, Atmos. Environ., 37, 3605-3613, 10.1016/s1352-2310(03)00326-1, 2003.

Liu, P., Ding, J., Liu, L., Xu, W., and Liu, X. J.: Estimation of surface ammonia concentrations and emissions in China from the polar-orbiting Infrared Atmospheric Sounding Interferometer and the FY-4A Geostationary Interferometric Infrared Sounder, Atmos. Chem. Phys., 22, 9099-9110, 10.5194/acp-22-9099-2022, 2022.

Ma, S. Y.: High-resolution assessment of ammonia emissions in China: Inventories, driving forces and mitigation, Atmos. Environ., 229, 10, 10.1016/j.atmosenv.2020.117458, 2020.

Morrison, H. and Milbrandt, J. A.: Parameterization of Cloud Microphysics Based on the Prediction of Bulk Ice Particle Properties. Part I: Scheme Description and Idealized Tests, J. Atmos. Sci., 72, 287-311, 10.1175/jas-d-14-0065.1, 2015.

Okita, T., Hara, H., and Fukuzaki, N.: Measurements of atmospheric SO_2 and SO_4^{2-}, and determination of the wet scavenging coefficient of sulfate aerosols for the winter monsoon season over the Sea of Japan, Atmos. Environ., 30, 3733-3739, 10.1016/1352-2310(96)00090-8, 1996.

Pruppacher, H. R. and Klett, J. D.: Microphysics of clouds and precipitation, Kluwer Academic Publishers, Dordrecht, Boston, London1997.

Seinfeld, J. H. and Pandis, S. N.: Atmospheric chemistry and physics: from air pollution to climate change, John Wiley & Sons2006.

Slinn, W. G. N., Randerson, D. (Ed.): Precipitation scavenging, in Atmospheric science power production, , Doc. DOE/TIC-27601, Tech. Inf. Cent., Off. Of Sci. and Tech. Inf., U.S. Dep. Of Energy, Washington, D.C.1984.

Sun, Y. L., Wang, Z. F., Du, W., Zhang, Q., Wang, Q. Q., Fu, P. Q., Pan, X. L., Li, J., Jayne, J., and Worsnop, D. R.: Long-term real-time measurements of aerosol particle composition in Beijing, China: seasonal variations, meteorological effects, and source analysis, Atmos. Chem. Phys., 15, 10149-10165, 10.5194/acp-15-10149-2015, 2015.

Tang, J., Xu, X. B., Ba, J., and Wang, S. F.: Trends of the precipitation acidity over China during 1992-2006, Chin. Sci. Bull., 55, 1800-1807, 10.1007/s11434-009-3618-1, 2010.

Wang, X., Zhang, L., and Moran, M. D.: Uncertainty assessment of current size-resolved parameterizations for below-cloud particle scavenging by rain, Atmos. Chem. Phys., 10, 5685-5705, 10.5194/acp-10-5685-2010, 2010.

Xiong, F. L.: Study of Fitting Gamma Raindrop Size Distribution (in Chinese), Master, Nanjing University of Information Science and Technology, 2016.

Xu, D. H., Ge, B. Z., Chen, X. S., Sun, Y. L., Cheng, N. L., Li, M., Pan, X. L., Ma, Z. Q., Pan, Y. P., and Wang, Z. F.: Multi-method determination of the below-cloud wet scavenging coefficients of aerosols in Beijing, China, Atmos. Chem. Phys., 19, 15569-15581, 10.5194/acp-19-15569-2019, 2019.

Xu, D. H., Ge, B. Z., Wang, Z. F., Sun, Y. L., Chen, Y., Ji, D. S., Yang, T., Ma, Z. Q., Cheng, N. L., Hao, J. Q., and Yao, X. F.: Below-cloud wet scavenging of soluble inorganic ions by rain in Beijing during the summer of 2014, Environ. Pollut., 230, 963-973, 10.1016/j.envpol.2017.07.033, 2017.

Zhang, X. M., Wu, Y. Y., Liu, X. J., Reis, S., Jin, J. X., Dragosits, U., Van Damme, M., Clarisse, L., Whitburn, S., Coheur, P. F., and Gu, B. J.: Ammonia Emissions May Be Substantially Underestimated in China, Environ. Sci. Technol., 51, 12089-12096, 10.1021/acs.est.7b02171, 2017.